TISSUE ENGINEERING: Part C
Volume 22, Number 11, 2016

DOI: 10.1089/ten.tec.2016.0253

termis
Tissue Engineering
& Regenerative Medicine
International Society

METHODS ARTICLE

Imaging of Hydrogel Microsphere Structure and Foreign Body Response Based on Endogenous X-Ray Phase Contrast

Alyssa A. Appel, MS,[1,2] Veronica Ibarra,[1] Sami I. Somo, MS,[1] Jeffery C. Larson, BS,[1,2]
Alfred B. Garson III, PhD,[3] Huifeng Guan, BS,[3] John Patrick McQuilling, BS,[4] Zhong Zhong, PhD,[5]
Mark A. Anastasio, PhD,[3] Emmanuel C. Opara, PhD,[4] and Eric M. Brey, PhD[1,2]

Transplantation of functional islets encapsulated in stable biomaterials has the potential to cure Type I diabetes. However, the success of these materials requires the ability to quantitatively evaluate their stability. Imaging techniques that enable monitoring of biomaterial performance are *critical* to further development in the field. X-ray phase-contrast (XPC) imaging is an emerging class of X-ray techniques that have shown significant promise for imaging biomaterial and soft tissue structures. In this study, XPC imaging techniques are shown to enable three dimensional (3D) imaging and evaluation of islet volume, alginate hydrogel structure, and local soft tissue features *ex vivo*. Rat islets were encapsulated in sterile ultrapurified alginate systems produced using a high-throughput microfluidic system. The encapsulated islets were implanted in omentum pouches created in a rodent model of type 1 diabetes. Microbeads were imaged with XPC imaging before implantation and as whole tissue samples after explantation from the animals. XPC microcomputed tomography (μCT) was performed with systems using tube-based and synchrotron X-ray sources. Islets could be identified within alginate beads and the islet volume was quantified in the synchrotron-based μCT volumes. Omental adipose tissue could be distinguished from inflammatory regions resulting from implanted beads in harvested samples with both XPC imaging techniques. Individual beads and the local encapsulation response were observed and quantified using quantitative measurements, which showed good agreement with histology. The 3D structure of the microbeads could be characterized with XPC imaging and failed beads could also be identified. These results point to the substantial potential of XPC imaging as a tool for imaging biomaterials in small animal models and deliver a critical step toward *in vivo* imaging.

Keywords: MicroCT, X-ray phase contrast, alginate hydrogel, analyzer-based imaging

Introduction

Biomaterial-based transplantation of healthy cells has been investigated for decades as a treatment for a number of disease states.[1–3] Research has primarily focused on islet encapsulation to treat type I diabetes.[4] Transplanted naked (not biomaterial encapsulated) islets have been shown to restore essential endocrine function, indicating that the transplantation of properly functioning endocrine cells into diseased patients can enhance overall metabolic function.[5,6] Immunoisolation of these cells in appropriately designed biomaterials could reduce or completely eliminate the need for immunosuppressant therapies.[4] However, the success of biomaterial-encapsulated cells requires that the microcapsules sustain their structure and stability *in vivo*.

Hydrogels are a class of biomaterials that have been investigated extensively for encapsulation of islets because of their ability to mimic the high water content and mechanical properties of soft tissue. Alginate-based materials have been popular materials for cell encapsulation and evaluated in

[1]Department of Biomedical Engineering, Illinois Institute of Technology, Chicago, Illinois.
[2]Research Services, Edward Hines Jr. VA Hospital, Chicago, Illinois.
[3]Department of Biomedical Engineering, Washington University in St. Louis, St. Louis, Missouri.
[4]Wake Forest Institute of Regenerative Medicine, Winston-Salem, North Carolina.
[5]National Synchrotron Light Source, Brookhaven National Laboratory, Upton, New York.

clinical trials for treatment of type I diabetes.[4,7–11] However, there are significant concerns with the stability and reproducibility of these systems.[7,12] A number of possible failure mechanisms have been proposed including poor cell survival because of an enhanced foreign body response, incomplete immunoisolation, and poor biomaterial stability.[13–23] Most *in vivo* studies rely on detection of blood glucose or C-peptide levels as indirect measures of stability, but these do not give insight into the actual mechanism of graft failure.[4,9,24] Histological and immunohistochemical methods are also frequently used but are invasive and destructive, do not allow for three dimensional (3D) assessment of the sample, often alter biomaterial structure, and require processing and staining techniques.[4,24–29]

There is a need for noninvasive imaging that allows for 3D assessment of the implanted grafts and local tissue response to monitor and predict long-term success of the transplant. The ideal imaging technique would not require exogenous contrast and be nondestructive. X-ray phase-contrast (XPC) imaging is a class of X-ray-based techniques that enable imaging of biomaterial and soft tissue structures,[30–35] which are difficult to observe using other imaging modalities. These techniques enable high-resolution and large volume imaging of these samples in the absence of exogenous contrast agents.

In this study, we provide evidence that XPC imaging techniques enable 3D imaging and evaluation of islet volume, alginate hydrogel structure, and local soft tissue response in explanted samples. Two XPC imaging techniques were used and both preimplantation and postimplantation samples were imaged. The first XPC imaging technique used a synchrotron X-ray source and is known as multiple image radiography (MIR). MIR is an analyzer-based XPC imaging method that results in reconstructed images representing the X-ray absorption, refraction, and ultrasmall-angle-X-ray-scatter (USAXS) properties of the samples.[36] MIR enables the identification of subtle material or tissue features based on complementary contrast mechanisms. However, synchrotron sources cannot be used for benchtop X-ray imaging. Therefore, we investigated a propagation-based XPC imaging method using a laboratory-scale X-ray tube source to demonstrate the translation of our XPC imaging findings to a broadly applicable in-laboratory system.

Materials and Methods

Extra samples from a previously published study including whole fixed explanted omentum-containing islet-encapsulated alginate microbeads and islet-encapsulated alginate microbeads preimplantation were provided by the Wake Forest Institute of Regenerative Medicine.[28]

Low-viscosity high-mannuronic acid (LVM) alginate (20–200 mPas; Nova-Matrix, Sandvika, Norway) was dissolved in 1.5% Eagle's minimum essential medium (MEM; Sigma-Aldrich, St. Louis, MO). Poly-L-ornithine (PLO; 30–70 kDa, Sigma-Aldrich), sodium citrate (Sigma-Aldrich), ultrapurified low-viscosity high-guluronic acid (LVG) alginate (75–200 kDa, G/M ratio ≤1), and LVM alginate (75–200 kDa, G/M ratio ≥1.5; Nova-Matrix, Sandvika, Norway) were also prepared in MEM. Cross-linking (100 mM $CaCl_2$) and wash (0.9% NaCl) solutions were prepared in deionized water. Fifty milligrams Dithizone (Sigma-Aldrich, St. Louis, MO) was dissolved in 5 mL of DMSO and mixed for 15 min. Fifteen milliliter Hank's balanced salt solution was added to the solution and mixed for an additional 15 min before filtering through a 0.45 μm filter syringe.

Animals

Approval by the Wake Forest University Institutional Animal Care and Use Committee (IACUC) was received before all animal studies.

Islet isolation and microencapsulation

Male Lewis and Wistar-Furth rats (250–300 g) (Harlan) were used as the source of islets for both isograft and allograft conditions. Islets were isolated from the pancreata of the rats using the standard procedure of collagenase digestion of pancreatic tissue[37] with modifications as described previously.[38] Purified islets were cultured overnight in RPMI-1640 medium (Sigma-Aldrich, 10% fetal bovine serum,10 mM HEPES).

The islets were encapsulated in an alginate/PLO/alginate microbeads using a modified[39] microfluidic procedure.[40] Islets were pelleted at 200 g (1 min, 4°C) and dispersed in 1.5% LVM alginate solution at 2000 islets/mL. Using a high-throughput flow-focusing microfluidic device at 1.4 psi, the islet suspension was pumped into the $CaCl_2$ crosslinking solution at a constant flow rate of 1.4 mL/min.[41] The alginate microbeads were incubated in this solution for 15 min and then washed before incubation in the 0.1% PLO solution for 20 min. To apply a uniform semipermeable PLO coating, gentle rotational mixing was employed during incubation in the PLO solution. The microbeads were incubated in 55 mM sodium citrate solution for 2 min. The outer layer of alginate was applied using 1.25% LVG solution for 5 min and followed by $CaCl_2$ (22 mM) solution crosslinking. The multilayer microbeads were washed with 2 mM $CaCl_2$ and then with normal saline. The islet-containing microbeads were cultured in RPMI-1640 medium before transplantation the next day.

In vivo *procedures*

Rodent model of type 1 diabetes. A week after arrival, diabetes was induced in Lewis rats (350–400 g) with an intraperitoneal injection of Streptozotocin (65 mg of STZ/kg). Blood glucose was monitored daily using a glucometer. The animals were considered diabetic when glucose levels were more than 400 mg/dL for two consecutive days.[42] Insulin pellets (Linshin, Canada) were inserted subcutaneously to maintain the health of the rats for at least 1 week before islet transplantation.

Microcapsule transplantation. Alginate-encapsulated microbeads were implanted in a rat omentum pouch model as described previously.[43] In brief, isoflurane was used for anesthesia, the abdominal area was shaved, cleaned, and disinfected, and a small incision was made below the stomach. Omental tissue was created into a pouch and the microbeads were placed in the pouch, which was then closed with suture before being returned to the peritoneal cavity (Fig. 1a).

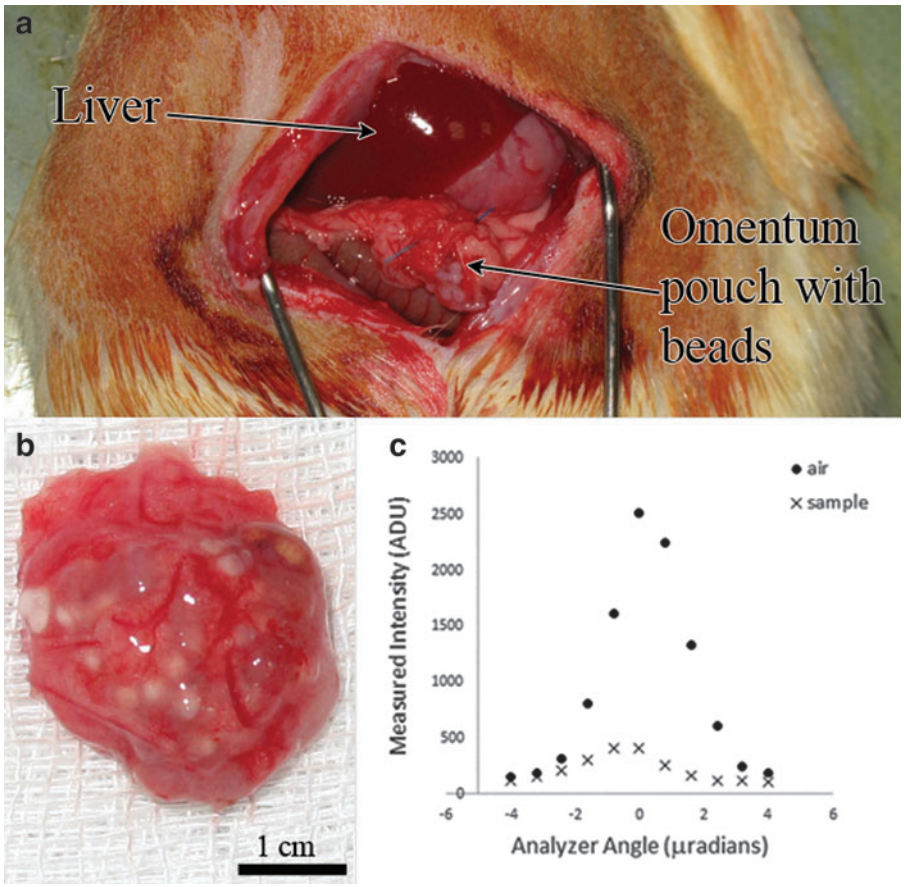

FIG. 1. **(a)** Photograph of rodent omentum pouch model. Pouch containing alginate microbeads can be seen in abdomen (*arrow*). **(b)** Photograph of explanted omentum pouch containing alginate microbeads. Example of sample that was imaged. **(c)** Example of rocking curves acquired in the absence (●) and presence (x) of omentum sample. Color images available online at www.liebertpub.com/tec

Approximately 800 islets were transplanted (~2000 islets/kg) in each recipient. All animals in the studies were given morphine after surgery and placed on a standard chow diet. After transplantation, if two consecutive blood glucose measurements in any recipient were more than 400 mg/dL, 10 U/kg of insulin was administered. Animals were euthanized and the omentum pouches containing the microbeads were explanted and fixed. Formalin has been shown to have a minimal effect on tissue properties determined by XPC imaging systems.[44]

XPC imaging

Synchrotron analyzer-based XPC imaging. Alginate microbeads containing islets and formalin-fixed whole explanted omentum pouches (Fig. 1b) were imaged submerged in calcium chloride solution using an XPC MIR imaging system at the National Synchrotron Light Source at Brookhaven National Laboratory (Beamline X15A).[45] X-ray imaging was performed using the following conditions: monochromated 20 keV beam, imager detector VHR 1:1, CCD sensor (Photonic Science Limited, United Kingdom; 400 × 4008 pixels, 9 μm resolution), and [333] analyzer crystal reflection. Measurement data were acquired from −4 to +4 μrad (total 11 analyzer crystal positions) to generate a rocking curve at each tomographic view angle (Fig. 1c).[46–48] A total of 500 tomographic views were acquired over 180° (1 s/angle). At each angle, the parametric MIR images representing the samples projected absorption, refraction, and USAXS properties were computed.[36] With the absorption, refraction, and USAXS images, we employed a filtered backprojection algorithm to reconstruct volumetric images. MATLAB R2012a (Mathworks) was used for reconstruction and image analysis. The rendering software was V3D.

Benchtop propagation-based XPC imaging. The benchtop propagation-based system used has been described in detail previously.[49] The explanted omenta-containing alginate beads were 38.7 cm from the source and 154.9 cm from the detector (5× magnification). The X-ray tube voltage was set at 60 kVp and current of 168 μA (nominal focal spot size = 12 μm, effective pixel size = 3 μm). The exposure time per view angle was 54 s. One hundred eighty-six tomographic views were collected with 1° of rotation between them. An OS-SART-FISTA reconstruction method (binning factor = 2)[50] was employed to reconstruct volumetric images of the sample (final spatial resolution = 24 μm). A total variation penalty was employed to balance the denoising effect and the fit of the solution to the data using a regularized least square optimization reconstruction problem. An adaptation of this algorithm was also employed for reconstructing tomosynthesis images using 40 view angles. The flexibility with regard to the measurement geometry and ability to mitigate data incompleteness makes iterative reconstruction algorithms more suited to the tomosynthesis problem.[51]

Histology

The omentum pouches were dehydrated in an ethanol series and paraffin embedded. Using a Leica RM2200 microtome, 5 μm serial sections were cut and stained with

Masson's trichrome or hematoxylin and eosin (H&E) using standard staining protocols. Section imaging was performed using an Axiovert 200 inverted microscope (Carl Zeiss MicroImaging, Inc. Gottingen, Germany) equipped with an AxioCam MRc5 color digital camera (Carl Zeiss). Tiling of multiple images enabled the generation of high-resolution (1.08 μm/pixel) images of entire cross sections using Axiovision 4.2 image analysis software (Carl Zeiss). Tissue sections were registered to reconstructed XPC microcomputed tomography (μCT) slices based on gross morphological structures that were easily identifiable in both XPC and histological images.

Quantification and analysis

Encapsulation thickness around individual beads was measured from XPC and histology images. The thickness of the tissue surrounding the alginate microbeads was clearly identified. At least eight measurements were made and averaged for at least 10 alginate microbeads. All data are expressed as means ± standard deviations with statistical comparisons performed using Student's *t*-test ($p \leq 0.05$ considered significant).

Results

XPC of microbeads preimplantation

Islets were isolated from rat pancreata and encapsulated in alginate microbeads prepared under sterile conditions. The alginate microbeads were imaged before implantation with MIR XPC to observe the biomaterial and islet structure. Under the imaging conditions, the microbeads were invisible in the absorption radiograph because of virtually no difference in X-ray absorption properties between the hydrogel and surrounding solution (Fig. 2a), but their structure could be clearly identified in refraction and USAXS images (Fig. 2b, c). Refraction CT slices of the beads allowed observation of the alginate bead structure and islets within the beads. Bead morphology was qualitatively consistent with images acquired from brightfield microscopy (Fig. 3a, b). The XPC images allowed for the identification of imperfections within the bead structure and on the surface, possibly resulting from the microfluidic system used for encapsulation. These features are often actively avoided as they are thought to play an important role in graft failure after transplantation.[15,18,52] The islets themselves were also identifiable in the microbeads. Volume rendering of the refraction images enabled observation of the spatial organization of islets (blue) inside the bead structure (green) (Fig. 3c).

Islet volume is often used as an indication of survival or success of transplanted cells, and the ability to image this volume in the biomaterial environment is a critical feature of an imaging tool.[53,54] Quantitative data can be extracted from the XPC μCT volume images, allowing determination of islet volume in the beads. The mean volume determined from XPC refraction images was $1.7 \pm 0.08 \times 10^5$ μm^3. These results cannot be directly compared with the measurements of islet area from 2D widefield optical microscopy ($5.8 \pm 3.1 \times 10^3$ μm^2). However, if islets are assumed to be spheres, these data result in XPC imaging radii of 34.4 μm in comparison with 43.2 μm from the microscopy images.

Synchrotron XPC imaging of microbeads in tissue

The microbeads were implanted in an omentum pouch model to evaluate stability and tissue response. Samples were explanted and XPC μCT was performed with an MIR XPC imaging technique followed by histology. Reconstructed MIR μCT slices display gross sample structure that is similar to histology (Fig. 4a–d). The adipose tissue of the surrounding omentum could be identified in both the absorption and refraction images (Fig. 4a, b). The large volume of alginate microbeads could be seen within the sample with individual microbeads clearly identified in the refraction images and in the 3D volume rendering of the sample (Fig. 4b, e and Supplementary Movies S1 and S2; Supplementary Data are available online at www.liebertpub.com/tec).

At higher magnification, individual beads generated contrast in refraction images that enabled evaluation of the local

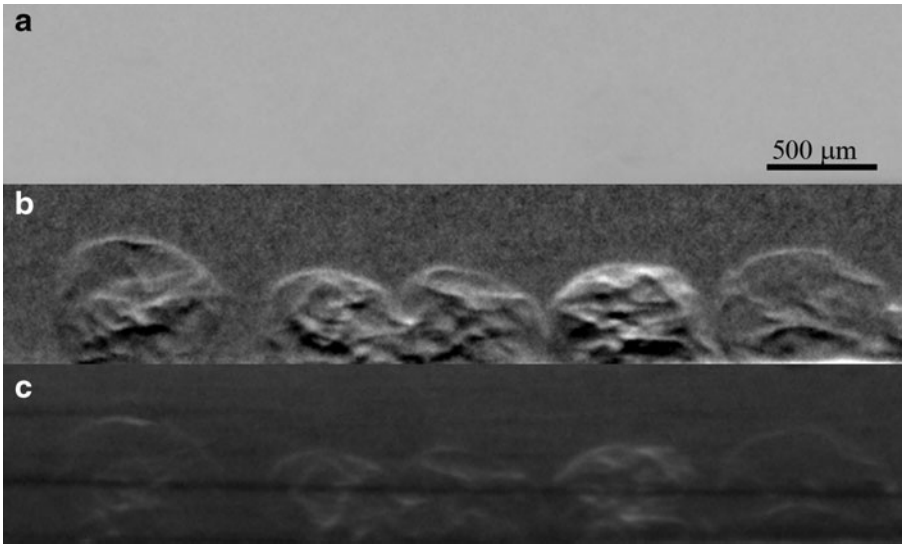

FIG. 2. Microbead structure generates contrast based on X-ray refraction and USAXS. MIR XPC allows reconstruction of **(a)** absorption **(b),** refraction, and **(c)** USAXS radiographs of alginate beads before implantation. Imperfections (wrinkles, folds) in the alginate structure can be identified within the refraction image. MIR, multiple image radiography; XPC, X-ray phase-contrast imaging; USAXS, ultrasmall-angle-X-ray-scatter.

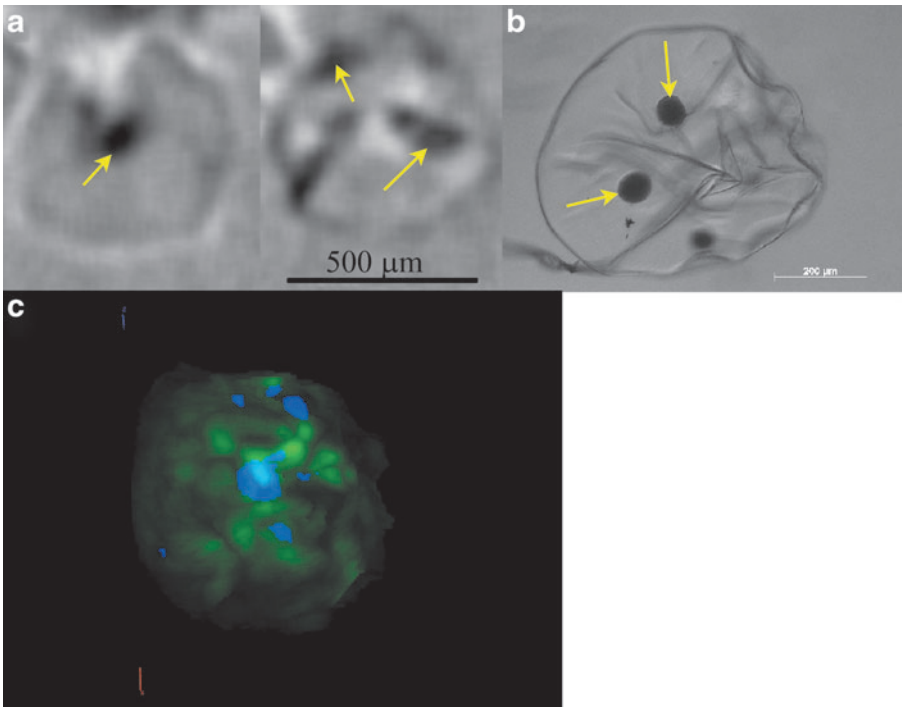

FIG. 3. Islets encapsulated within alginate microbeads can be imaged with XPC μCT. **(a)** Reconstructed X-ray refraction μCT slices showing islets (*arrows*) within the beads. The structure looks similar to **(b)** a brightfield microscopy image. **(c)** The refraction CT images can be reconstructed to generate a pseudocolored volume rendering showing the spatial organization of encapsulated islets (*blue*) within the alginate microbeads (*green*). μCT, microcomputed tomography. Color images available online at www.liebertpub.com/tec

structure. The bead and soft tissue structure observed in XPC images matched well with histology (Fig. 5a–d). Both failed beads exhibiting invasion by soft tissue (Fig. 5a, b) and intact beads surrounded by a layer of encapsulation tissue (Fig. 5c, d) could be identified in regions of interest from the whole sections (Fig. 4b, d). As expected, the hydrogel structure in the histology exhibited distortions because of processing, resulting in separation from the surrounding soft tissue (Fig. 5c). However, the layer of encapsulation tissue that is clearly maintained in the

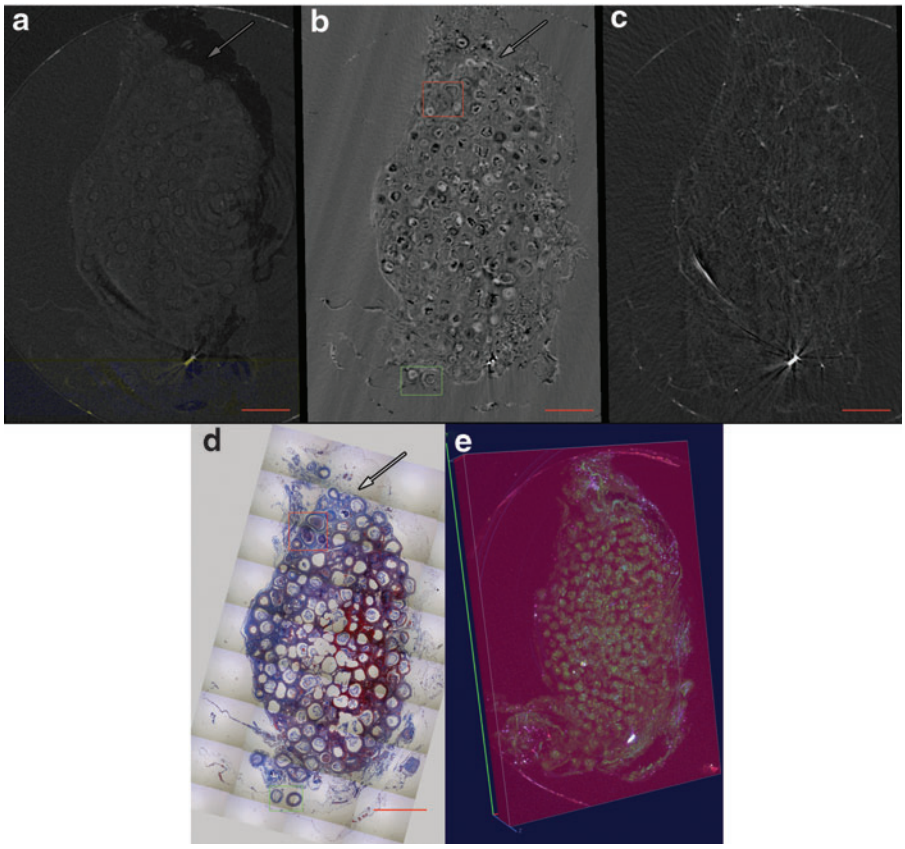

FIG. 4. MIR CT slice of the omentum sample showing **(a)** absorption, **(b)** refraction, **(c)** and USAXS images. The samples were processed and stained for **(d)** Masson trichrome, showing a similar structure of the images. *Arrows* indicate adipose tissue. Scale bar = 2.25 mm. **(e)** 3D renderings of rat omentum-containing alginate beads. *Red* represents absorption, *green* represents refraction, and *blue* represents USAXS. 3D, three dimensional. Color images available online at www.liebertpub.com/tec

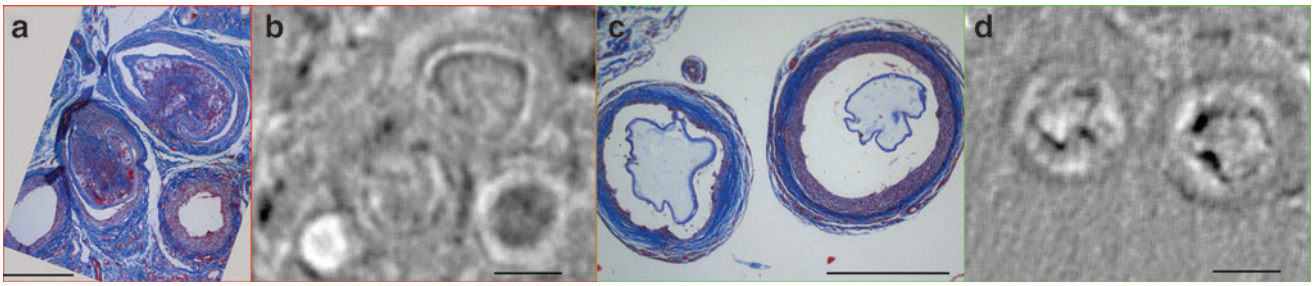

FIG. 5. The structure of both failed and intact alginate microbeads could be identified within the XPC refraction images with strong agreement with findings from histology. **(a, c)** Magnified regions of Masson's trichrome stains of Figure 4d and (**b, d**) corresponding regions of interest from XPC refraction image in Figure 4b of **(a, b)** failed (invaded) and **(c, d)** intact beads. Scale bar = 0.45 mm. Color images available online at www.liebertpub.com/tec

histological staining was also identified in the XPC images. This layer is of critical importance in determining the function of the implanted cells as it regulates communication with the host tissue.

The fibrous encapsulation layer was also clearly visible around beads in coronal plane refraction CT slices (Fig. 6a). There is a clear distinction between this encapsulation surrounding the beads and the rest of the fibrovascular tissue that allowed for quantification of this tissue thickness. The XPC measurements showed good agreement with measurements determined by use of the gold standard method, histology (Fig. 6e). There was no difference between the tissue thickness measured in the refraction images and H&E sections. The bead structure and shape can also clearly be seen. In another sample, a low encapsulation response was observed, resulting in improved biomaterial integration. In this sample, the adipose tissue and beads were visible but the encapsulation layer was not observed, and a more homogeneous tissue was present representative of a healing response (Fig. 6c, d).

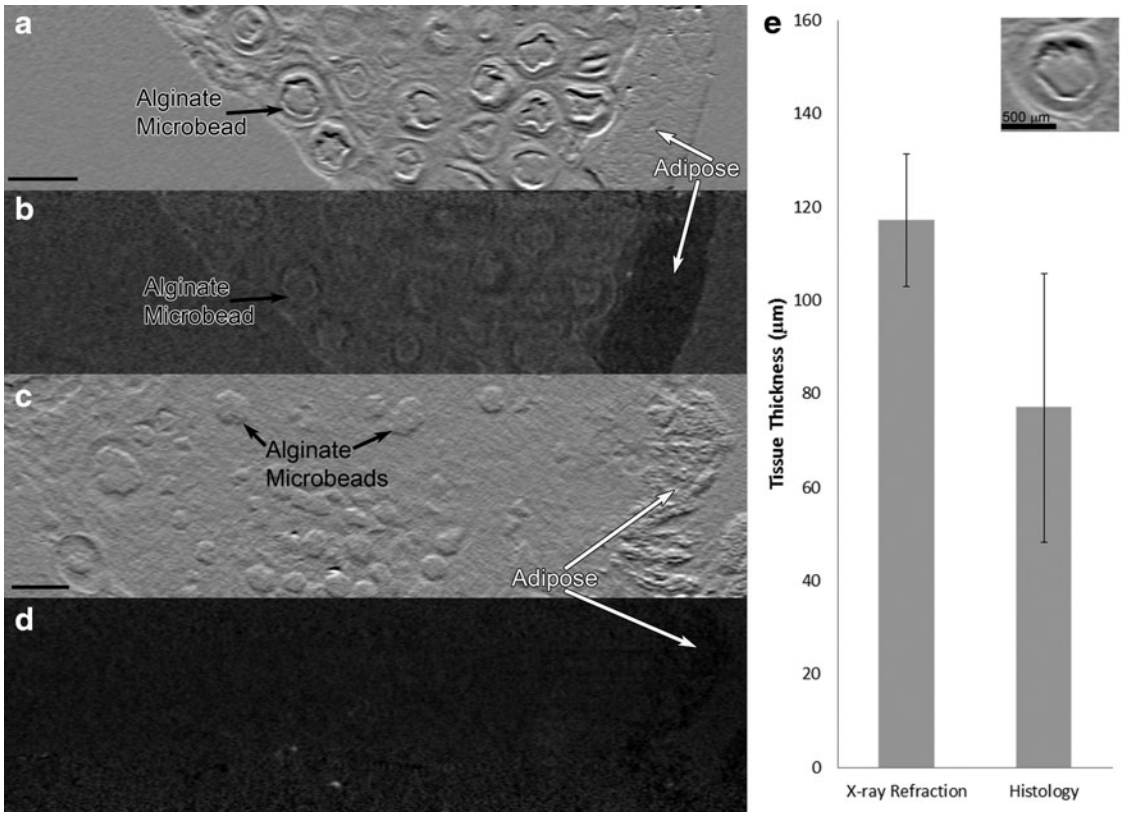

FIG. 6. XPC imaging can differentiate between implanted microbeads generating a foreign body encapsulation response **(a, b)** and a healing **(c, d)** response to implanted biomaterials. Coronal plane CT images are shown for **(a, c)** refraction and **(b, d)** absorption CT slices. Adipose, *white arrows*, can be identified in both absorption and refraction images but only the refraction images allow observation of the individual beads, *black arrows*. Scale bar = 1 mm. **(e)** Thickness of encapsulation response around alginate microbeads measured in both MIR refraction images and H&E sections. *Inset* shows a coronal plane refraction CT image of an individual bead with a layer of fibrous encapsulation. H&E, hematoxylin and eosin.

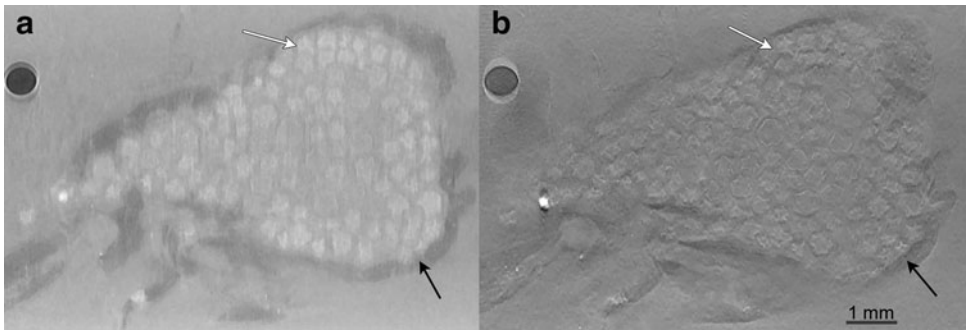

FIG. 7. Propagation-based XPC imaging enables imaging of soft tissue, biomaterial structure, and encapsulation response in the tissue samples. Images of an omentum with alginate microbeads reconstructed with **(a)** 186 views using OS- SART-FISTA reconstruction algorithm and **(b)** 40 views using a tomosynthesis reconstruction algorithm show similar detail. *Black arrows* indicate surrounding adipose tissue from omentum and *white arrows* point to fibrovascular tissue formed in response to the microbeads.

Tube-based XPC imaging of microbeads in tissue

XPC μCT of tissue samples was also performed using a benchtop system using an X-ray tube source. This propagation-based XPC implementation results in a single image that is a combination of the contrast mechanisms exhibited in the three MIR images. The gross morphology of the sample could be clearly identified with propagation XPC μCT (Fig. 7a). The adipose tissue from the surrounding omentum was distinguishable from the tissue and microbeads in the center of the tissue. The alginate microbeads were also clearly discernable within the tissue (Fig. 7a). To gain insight into the potential of imaging under more constrained conditions, a tomosynthesis reconstruction algorithm that used a limited number of views was implemented for comparison with the full view reconstruction (Fig. 7b). Similar image details were visible in the corresponding limited view CT slice as seen in the full view reconstruction.

The bead shape and structure as well as the local encapsulation response identified in the XPC images matched well with findings from histological stains (Fig. 8a–c). The tissue thickness surrounding the beads could be quantified from the XPC images and the values were not significantly different from the thickness values determined from histological stains (Fig. 8d).

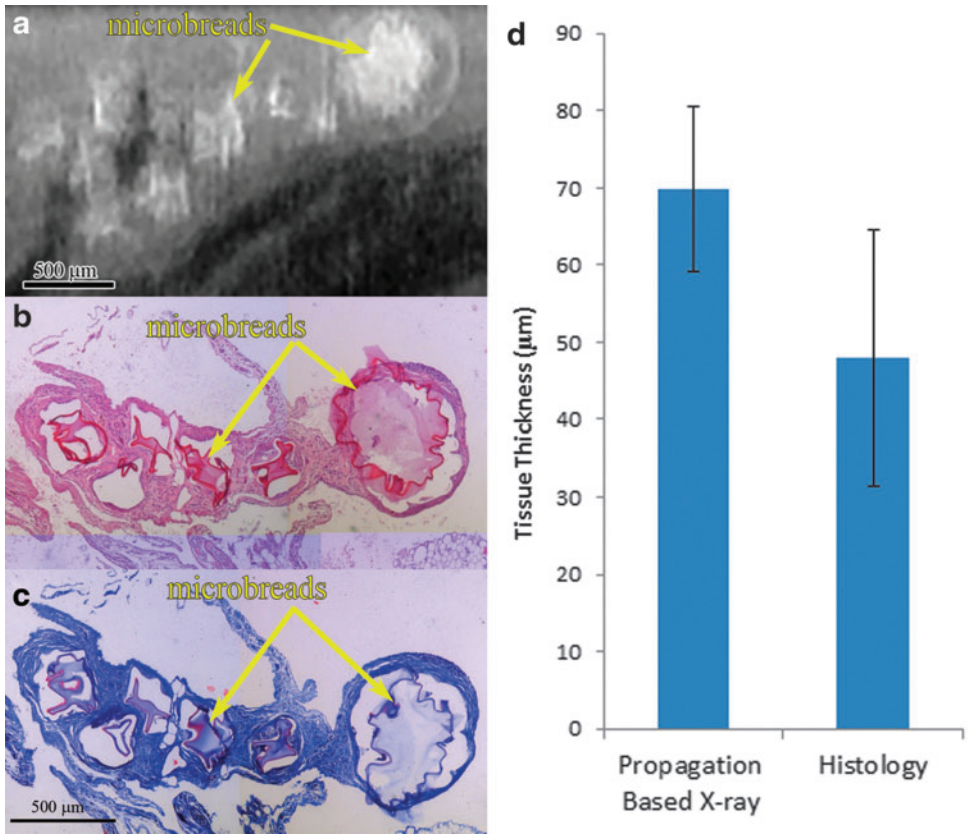

FIG. 8. Region of interest of an omentum with alginate microbeads, *yellow arrows* **(a)** XPC image with corresponding **(b)** H&E and **(c)** Masson trichrome sections with **(d)** graph of tissue thickness of encapsulation response around alginate microbeads in propagation-based XPC images and H&E sections. Color images available online at www.liebertpub.com/tec

Discussion

There is a critical need for noninvasive, nondestructive tools that enable 3D assessment of biomaterial structure and soft tissue structure to further develop tissue engineering and cellular therapies. These tools are necessary both for preimplant evaluation as a screening method and for implantation monitoring to assess the local tissue response and stability of the biomaterials. XPC imaging is a developing category of X-ray techniques that have shown significant potential for imaging biomaterial and soft tissue structures that are difficult to observe with other imaging modalities. Specifically, these techniques have been successful in observing hydrogels in tissue[30,31,35] and low-density scaffolds in water[46] and soft tissue.[33,34] The techniques enable high-resolution, large volume imaging of these materials, without the need for exogenous contrast agents. In this study, we expanded on previous XPC studies, and found that XPC μCT enabled assessment of bead shape and structure before implantation. The ability to observe imperfections in bead structure is important as bead morphology can lead to poor biocompatibility of the capsules. Spherical beads are ideal and deviation from this shape can result in a poor healing response and contribute to graft failure.[18,52] XPC imaging also allowed observation of the spatial orientation of islets within the beads and allowed quantification of islet size. Islet volume is an important indicator of islet function and viability. The ability to monitor, quantitatively, islet volume within encapsulation systems has been proposed as a method for tracking islet survival and function.[53,54] Our results suggest that further development of XPC for *in vivo* imaging could provide an important new tool for monitoring encapsulated islets.

XPC μCT was successful in imaging the structure of alginate microcapsules within tissue. Both failed beads that had been invaded by inflammatory tissue and intact microbeads could be identified in the X-ray refraction images. The structures matched well with histological images but without the destructive sectioning and processing artifacts. These findings demonstrate the power of XPC techniques for evaluating whole volume tissue samples with nondestructive methods and the potential for future monitoring of graft failure.

Many other medical imaging modalities have been employed for noninvasive observation of microbead location. Magnetic resonance imaging (MRI), absorption-based X-ray CT, and ultrasound (US) imaging may enable identification of cell/graft location either alone or in combination.[55–61] To enhance image contrast, an additional agent is often incorporated within the cells or the alginate microbeads. Contrast agents that have been explored include iron oxide nanoparticles,[55,58,61] gold nanoparticles,[55,61] and perfluorocarbon (PFC) nanoparticles.[55,59,60] Some of these agents (e.g., iron oxide and gold nanoparticles) appear to be nontoxic, but their effect on the long-term islet function is unknown. Placing PFC emulsions into alginate microspheres leads to spheres that are readily observed with ^{19}F MR imaging, US, and CT, increased *in vitro* insulin secretion, and enabled prolonged *in vivo* insulin secretion.[59,62]

The strategy of incorporating contrast agents in the biomaterial may also allow for monitoring of mechanical stability *in vivo*.[55] Conceptually, microbead breakdown would result in dispersion of the contrast agent and altered signal intensity. However, signal changes have not been shown to quantitatively correlate with bead breakdown. These previous imaging studies represent progress toward the long-term monitoring of implanted grafts. However, the requirement of contrast agents limits application and the techniques did not provide information on local tissue response. The local tissue response is critical to success of the grafts. Using magnetic transfer ratio MRI images, Chan *et al.* quantified differences in local immune response to implanted alginate microbeads both with and without cells and in the presence and absence of immunosuppression therapy.[63] This study demonstrated how MRI can be used to detect variances in the local response to the implant.

In many situations, stable biomaterials may still fail because of the response of the tissue after implantation. A poor foreign body response resulting in either chronic inflammation or a thick layer of avascular encapsulation tissue can hinder communication between the encapsulated cells and host tissue. XPC imaging provides the ability to quantify the encapsulation thickness surrounding the beads. In addition, in samples in which beads showed good integration with host tissues, the homogeneous healing tissue was visually distinct from the encapsulation response observed in the histologically more complex inflammatory tissue.

Two different XPC techniques were used in this research. MIR XPC imaging provided the greater detail on the contrast mechanisms of the material and tissue by providing separate images, depicting the X-ray absorption, refraction, and USAXS properties. MIR XPC μCT also allowed for observation of islets within the microbeads and quantification of their volume. However, the requirement of a monochromatic X-ray beam primarily limits application to a synchrotron light source. The potential application of the MIR XPC method for routine use in laboratory imaging is impractical. Alternatively, a propagation-based, in-laboratory system using a microfocus X-ray tube is a more accessible form of XPC imaging. When the samples were imaged with an in-laboratory propagation-based XPC system, sample features were identified similar to the synchrotron-based system. The application of this system involves a standard microfocus X-ray source and detector leading to relatively easy implementation and wide accessibility. Furthermore, a limited view reconstruction algorithm was implemented, resulting in image quality similar to the full view reconstruction. This demonstrated that similar features can be seen with a shorter scan time and lower dose, providing support for the eventual application of XPC for noninvasive animal imaging.

Conclusion

We have successfully imaged alginate beads in soft tissue using both synchrotron and benchtop implementations of XPC imaging. The MIR XPC imaging technique allowed for 3D assessment of bead shape and islet volume before implantation without altering or destroying the samples unlike standard histological methods. These methods allowed for the evaluation of tissue formed in response to the grafts and observation of biomaterial structure within the tissue. These results provide a preview into the substantial potential use of XPC techniques to observe and characterize biomaterial

structure and tissue response to implanted biomaterials and demonstrate a critical step toward *in vivo* imaging.

Acknowledgments

The authors thank Rajesh Pareta and Sittadjody Sivanandane for help with sample preparation. This research was funded by the National Science Foundation (EEC-1157041 and 1461215, CBET-1263994), the National Institute of Health (R01EB009715, 5R01EB020604-02), and the Veteran's Administration (5 I01 BX000418).

Disclosure Statement

No competing financial interests exist.

References

1. Tatard, V., Menei, P., Benoit, J., and Montero-Menei, C. Combining polymeric devices and stem cells for the treatment of neurological disorders: a promising therapeutic approach. Curr Drug Targets **6,** 81, 2005.
2. Assuncao-Silva, R.C., Gomes, E.D., Sousa, N., Silva, N.A., and Salgado, A.J. Hydrogels and cell based therapies in spinal cord injury regeneration. Stem Cells Int **2015,** 948040, 2015.
3. Cezar, C.A., and Mooney, D.J. Biomaterial-based delivery for skeletal muscle repair. Adv Drug Deliv Rev **84,** 188, 2015.
4. Scharp, D.W., and Marchetti, P. Encapsulated islets for diabetes therapy: history, current progress, and critical issues requiring solution. Adv Drug Deliv Rev **67–68,** 35, 2014.
5. McCall, M., and Shapiro, A.M. Update on islet transplantation. Cold Spring Harb Perspect Med **2**, a007823, 2012.
6. Ramesh, A., Chhabra, P., and Brayman, K. Pancreatic islet transplantation in type 1 diabetes mellitus: an update on recent developments. Curr Diabetes Rev **9**, 294, 2013.
7. Calafiore, R., and Basta, G. Clinical application of microencapsulated islets: actual prospectives on progress and challenges. Adv Drug Deliv Rev **67–68,** 84, 2014.
8. Calafiore, R., Basta, G., Luca, G., Lemmi, A., Montanucci, M.P., Calabrese, G., Racanicchi, L., Mancuso, F., and Brunetti, P. Microencapsulated pancreatic islet allografts into nonimmunosuppressed patients with type 1 diabetes. Diabetes Care **29,** 137, 2006.
9. Buder, B., Alexander, M., Krishnan, R., Chapman, D.W., and Lakey, J.R. Encapsulated islet transplantation: strategies and clinical trials. Immune Netw **13,** 235, 2013.
10. De Vos, P., Hamel, A., and Tatarkiewicz, K. Considerations for successful transplantation of encapsulated pancreatic islets. Diabetologia **45,** 159, 2002.
11. Elliott, R.B., Escobar, L., Tan, P.L., Muzina, M., Zwain, S., and Buchanan, C. Live encapsulated porcine islets from a type 1 diabetic patient 9.5 yr after xenotransplantation. Xenotransplantation **14,** 157, 2007.
12. Koellmer, M., Somo, S., Appel, A., and Brey, E.M. Long-term function of alginate encapsulated islets. Tissue Eng Part B **22,** 34, 2015.
13. Chen, H., Ouyang, W., Martoni, C., and Prakash, S. Genipin cross-linked polymeric alginate-chitosan microcapsules for oral delivery: in-vitro analysis. Int J Polym Sci **2009,** 1, 2009.
14. de Vos, P., van Hoogmoed, C.G., de Haan, B.J., and Busscher, H.J. Tissue responses against immunoisolating alginate-PLL capsules in the immediate posttransplant period. J Biomed Mater Res **62,** 430, 2002.
15. Dufrane, D., Goebbels, R.-M., Saliez, A., Guiot, Y., and Gianello, P. Six-month survival of microencapsulated pig islets and alginate biocompatibility in primates: proof of concept. Transplantation **81,** 1345, 2006.
16. Hillberg, A.L., Kathirgamanathan, K., Lam, J.B., Law, L.Y., Garkavenko, O., and Elliott, R.B. Improving alginate-poly-L-ornithine-alginate capsule biocompatibility through genipin crosslinking. J Biomed Mater Res B Appl Biomater **101,** 258, 2013.
17. Kim, A.R., Hwang, J.H., Kim, H.M., Kim, H.N., Song, J.E., Yang, Y.I., Yoon, K.H., Lee, D., and Khang, G. Reduction of inflammatory reaction in the use of purified alginate microcapsules. J Biomater Sci Polym Ed **24,** 1084, 2013.
18. Li, H.B., Jiang, H., Wang, C.Y., Duan, C.M., Ye, Y., Su, X.P., Kong, Q.X., Wu, J.F., and Guo, X.M. Comparison of two types of alginate microcapsules on stability and biocompatibility in vitro and in vivo. Biomed Mater **1,** 42, 2006.
19. Mallett, A.G., and Korbutt, G.S. Alginate modification improves long-term survival and function of transplanted encapsulated islets. Tissue Eng Part A **15,** 1301, 2008.
20. Schneider, S., and Klein, H.H. Long-term graft function of cryostored alginate encapsulated rat islets. Eur J Med Res **16,** 396, 2011.
21. Van Raamsdonk, J., Cornelius, R., Brash, J., and Chang, P. Deterioration of polyamino acid-coated alginate microcapsules in vivo. J Biomater Sci Polym Ed **13,** 863, 2002.
22. de Groot, M., Schuurs, T.A., and van Schilfgaarde, R. Causes of limited survival of microencapsulated pancreatic islet grafts. J Surg Res **121,** 141, 2004.
23. Van Schilfgaarde, R., and De Vos, P. Factors influencing the properties and performance of microcapsules for immunoprotection of pancreatic islets. J Mole Med **77,** 199, 1999.
24. Berman, D.M., O'Neil, J.J., Coffey, L.C., Chaffanjon, P.C., Kenyon, N.M., Ruiz, P., Jr., Pileggi, A., Ricordi, C., and Kenyon, N.S. Long-term survival of nonhuman primate islets implanted in an omental pouch on a biodegradable scaffold. Am J Transplant **9,** 91, 2009.
25. de Vos, P., van Hoogmoed, C.G., van Zanten, J., Netter, S., Strubbe, J.H., and Busscher, H.J. Long-term biocompatibility, chemistry, and function of microencapsulated pancreatic islets. Biomaterials **24,** 305, 2003.
26. Ibarra, V., Appel, A.A., Anastasio, M.A., Opara, E.C., and Brey, E.M. Evaluation of the tissue response to alginate encapsulated islets in an omentum pouch model. J Biomed Mater Res A **104,** 1581, 2016.
27. Kobayashi, T., Aomatsu, Y., Iwata, H., Kin, T., Kanehiro, H., Hisanga, M., Ko, S., Nagao, M., Harb, G., and Nakajima, Y. Survival of microencapsulated islets at 400 days posttransplantation in the omental pouch of NOD mice. Cell Transplant **15,** 359, 2006.
28. Pareta, R., McQuilling, J.P., Sittadjody, S., Jenkins, R., Bowden, S., Orlando, G., Farney, A.C., Brey, E.M., and Opara, E.C. Long-term function of islets encapsulated in a re-designed alginate microcapsule construct in omentum pouches of immune-competent diabetic rats. Pancreas **43,** 605, 2014.

29. Vériter, S., Mergen, J., Goebbels, R.-M., Aouassar, N., Grégoire, C., Jordan, B., Levêque, P., Gallez, B., Gianello, P., and Dufrane, D. In vivo selection of biocompatible alginates for islet encapsulation and subcutaneous transplantation. Tissue Eng Part A **16,** 1503, 2010.
30. Appel, A.A., Larson, J.C., Garson, A.B., 3rd, Guan, H., Zhong, Z., Nguyen, B.N., Fisher, J.P., Anastasio, M.A., and Brey, E.M. X-ray phase contrast imaging of calcified tissue and biomaterial structure in bioreactor engineered tissues. Biotechnol Bioeng **112,** 612, 2015.
31. Brey, E.M., Appel, A., Chiu, Y.C., Zhong, Z., Cheng, M.H., Engel, H., and Anastasio, M.A. X-ray imaging of poly(ethylene glycol) hydrogels without contrast agents. Tissue Eng Part C Methods **16,** 1597, 2010.
32. Cedola, A., Campi, G., Pelliccia, D., Bukreeva, I., Fratini, M., Burghammer, M., Rigon, L., Arfelli, F., Chang Chen, R., Dreossi, D., Sodini, N., Mohammadi, S., Tromba, G., Cancedda, R., and Mastrogiacomo, M. Three dimensional visualization of engineered bone and soft tissue by combined x-ray micro-diffraction and phase contrast tomography. Phys Med Biol **59,** 189, 2014.
33. Izadifar, Z., Chapman, L.D., and Chen, X. Computed tomography diffraction-enhanced imaging for in situ visualization of tissue scaffolds implanted in cartilage. Tissue Eng Part C Methods **20,** 140, 2014.
34. Zhu, N., Chapman, D., Cooper, D., Schreyer, D.J., and Chen, X. X-ray diffraction enhanced imaging as a novel method to visualize low-density scaffolds in soft tissue engineering. Tissue Eng Part C Methods **17,** 1071, 2011.
35. Appel, A.A., Larson, J.C., Jiang, B., Zhong, Z., Anastasio, M.A., and Brey, E.M. X-ray phase contrast allows three dimensional, quantitative imaging of hydrogel implants. Ann Biomed Eng **44,** 773, 2016.
36. Wernick, M.N., Wirjadi, O., Chapman, D., Zhong, Z., Galatsanos, N.P., Yang, Y., Brankov, J.G., Oltulu, O., Anastasio, M.A., and Muehleman, C. Multiple-image radiography. Phys Med Biol **48,** 3875, 2003.
37. Lacy, P., and Kostianovsky, M. Method for the isolation of intact islets from the pancreas. Diabetes **967,** 35.
38. Field, J., Farney, A., and Sutherland, D.E. Improved islet isolation from rat pancreas using 35% bovine serum albumin in combination with dextran gradient separation. Transplantation **61,** 1554, 1996.
39. Khanna, O., Moya, M.L., Opara, E.C., and Brey, E.M. Synthesis of multilayered alginate microcapsules for the sustained release of fibroblast growth factor-1. J Biomed Mater Res A **95,** 632, 2010.
40. Darrabie, M.D., Kendall, W.F., and Opara, E.C. Characteristics of poly-L-ornithine-coated alginate microcapsules. Biomaterials **26,** 6846, 2005.
41. Tendulkar, S., Mirmalek-Sani, S.-H., Childers, C., Saul, J., Opara, E.C., and Ramasubramanian, M.K. A three-dimensional microfluidic approach to scaling up microencapsulation of cells. Biomed Microdevices **14,** 461, 2012.
42. Goss, J.A., Flye, M.W., and Lacy, P.E. Induction of allogeneic islet survival by intrahepatic islet preimmunization and transient immunosuppression. Diabetes **45,** 144, 1996.
43. Khanna, O., Huang, J.J., Moya, M.L., Wu, C.W., Cheng, M.H., Opara, E.C., and Brey, E.M. FGF-1 delivery from multilayer alginate microbeads stimulates a rapid and persistent increase in vascular density. Microvasc Res **90,** 23, 2013.
44. Mollenhauer, J., Aurich, M.E., Zhong, Z., Muehleman, C., Cole, A.A., Hasnah, M., Oltulu, O., Kuettner, K.E., Margulis, A., and Chapman, L.D. Diffraction-enhanced X-ray imaging of articular cartilage. Osteoarthritis Cartilage **10,** 163, 2002.
45. Zhong, Z., Thomlinson, W., Chapman, D., and Sayers, D. Implementation of diffraction-enhanced imaging experiments: at the NSLS and APS. Nucl Instrum Methods Phys Res A **450,** 556, 2000.
46. Appel, A.A., Larson, J.C., Somo, S., Zhong, Z., Spicer, P.P., Kasper, F.K., Garson, A.B., 3rd, Zysk, A.M., Mikos, A.G., Anastasio, M.A., and Brey, E.M. Imaging of poly(alpha-hydroxy-ester) scaffolds with X-ray phase-contrast microcomputed tomography. Tissue Eng Part C Methods **18,** 859, 2012.
47. Brankov, J.G., Wernick, M.N., Yang, Y., Li, J., Muehleman, C., Zhong, Z., and Anastasio, M.A. A computed tomography implementation of multiple-image radiography. Med Phys **33,** 278, 2006.
48. Chou, C.-Y., Anastasio, M.A., Brankov, J.G., Wernick, M.N., Brey, E.M., Connor, D.M., and Zhong, Z. An extended diffraction-enhanced imaging method for implementing multiple-image radiography. Phys Med Biol **52,** 1923, 2007.
49. Zysk, A.M., Garson, A.B., 3rd, Xu, Q., Brey, E.M., Zhou, W., Brankov, J.G., Wernick, M.N., Kuszak, J.R., and Anastasio, M.A. Nondestructive volumetric imaging of tissue microstructure with benchtop x-ray phase-contrast tomography and critical point drying. Biomed Opt Express **3,** 1924, 2012.
50. Guan, H., Xu, Q., Garson, A., and Anastasio, M.A. Depth resolution properties of in-line X-ray phase-contrast tomosynthesis. Proc SPIE **9033,** 90330H, 2014.
51. Guan, H., Xu, Q., Garson, A.B., 3rd, and Anastasio, M.A. Boundary-enhancement in propagation-based x-ray phase-contrast tomosynthesis improves depth position characterization. Phys Med Biol **60,** N151, 2015.
52. de Vos, P., Spasojevic, M., de Haan, B.J., and Faas, M.M. The association between in vivo physicochemical changes and inflammatory responses against alginate based microcapsules. Biomaterials **33,** 5552, 2012.
53. Morini, S., Braun, M., Onori, P., Cicalese, L., Elias, G., Gaudio, E., and Rastellini, C. Morphological changes of isolated rat pancreatic islets: a structural, ultrastructural and morphometric study. J Anat **209,** 381, 2006.
54. Shin, J.S., Min, B.H., Lim, J.Y., Kim, B.K., Han, H.J., Yoon, K.H., Kim, S.J., and Park, C.G. Novel culture technique involving an histone deacetylase inhibitor reduces the marginal islet mass to correct streptozotocin-induced diabetes. Cell Transplant **20,** 1321, 2011.
55. Arifin, D.R., Kedziorek, D.A., Fu, Y., Chan, K.W., McMahon, M.T., Weiss, C.R., Kraitchman, D.L., and Bulte, J.W. Microencapsulated cell tracking. NMR Biomed **26,** 850, 2013.
56. Arifin, D.R., Long, C.M., Gilad, A.A., Alric, C., Roux, S., Tillement, O., Link, T.W., Arepally, A., and Bulte, J.W. Trimodal gadolinium-gold microcapsules containing pancreatic islet cells restore normoglycemia in diabetic mice and can be tracked by using US, CT, and positive-contrast MR imaging. Radiology **260,** 790, 2011.
57. Barnett, B., Kraitchman, D., Lauzon, C., Magee, C., Walczak, P., Gilson, W., Arepally, A., and Bulte, J. Radiopaque alginate microcapsules for X-ray visualization and immunoprotection of cellular therapeutics. Mol Pharm **3,** 531, 2006.

58. Barnett, B.P., Arepally, A., Karmarkar, P.V., Qian, D., Gilson, W.D., Walczak, P., Howland, V., Lawler, L., Lauzon, C., Stuber, M., Kraitchman, D.L., and Bulte, J.W. Magnetic resonance-guided, real-time targeted delivery and imaging of magnetocapsules immunoprotecting pancreatic islet cells. Nat Med **13,** 986, 2007.
59. Barnett, B.P., Ruiz-Cabello, J., Hota, P., Ouwerkerk, R., Shamblott, M.J., Lauzon, C., Walczak, P., Gilson, W.D., Chacko, V.P., Kraitchman, D.L., Arepally, A., and Bulte, J.W. Use of perfluorocarbon nanoparticles for non-invasive multimodal cell tracking of human pancreatic islets. Contrast Media Mol Imaging **6,** 251, 2011.
60. Cormode, D.P., Mulder, W.J., and Fayad, Z.A. Science to practice: versatile method to track transplanted encapsulated islet cells with multiple imaging modalities. Radiology **258,** 1, 2011.
61. Kim, J., Arifin, D.R., Muja, N., Kim, T., Gilad, A.A., Kim, H., Arepally, A., Hyeon, T., and Bulte, J.W. Multifunctional capsule-in-capsules for immunoprotection and trimodal imaging. Angew Chem Int Ed Engl **50,** 2317, 2011.
62. Barnett, B.P., Ruiz-Cabello, J., Hota, P., Liddell, R., Walczak, P., Howland, V., Chacko, V.P., Kraitchman, D.L., Arepally, A., and Bulte, J.W. Fluorocapsules for improved function, immunoprotection, and visualization of cellular therapeutics with MR, US, and CT Imaging 1. Radiology **258,** 182, 2011.
63. Chan, K.W., Liu, G., van Zijl, P.C., Bulte, J.W., and McMahon, M.T. Magnetization transfer contrast MRI for non-invasive assessment of innate and adaptive immune responses against alginate-encapsulated cells. Biomaterials **35,** 7811, 2014.

Address correspondence to:
Eric M. Brey, PhD
Department of Biomedical Engineering
Illinois Institute of Technology
3255 South Dearborn Street
Chicago, IL 60616

E-mail: brey@iit.edu

Mark A. Anastasio, PhD
Department of Biomedical Engineering
Washington University in St. Louis
One Brookings Drive
St. Louis, MO 63130

E-mail: anastasio@seas.wustl.edu

Received: June 24, 2016
Accepted: October 28, 2016
Online Publication Date: November 14, 2016